Vibronic effects in the spectroscopy and dynamics of *C*-phycocyanin

2012 J. Phys. B: At. Mol. Opt. Phys. 45 154016

(http://iopscience.iop.org/0953-4075/45/15/154016)

J. Phys. B: At. Mol. Opt. Phys. **45** (2012) 154016 (12pp) doi:10.1088/0953-4075/45/15/154016

Vibronic effects in the spectroscopy and dynamics of *C*-phycocyanin

Jordan M Womick[1], **Brantley A West**[2], **Norbert F Scherer**[3] **and Andrew M Moran**[1]

[1] Department of Chemistry, The University of North Carolina at Chapel Hill, Chapel Hill, NC 27599, USA
[2] Department of Physics and Astronomy, The University of North Carolina at Chapel Hill, Chapel Hill, NC 27599, USA
[3] Department of Chemistry and the James Franck Institute, The University of Chicago, Chicago, IL 60637, USA

E-mail: ammoran@email.unc.edu

Received 23 March 2012, in final form 31 May 2012
Published 30 July 2012
Online at stacks.iop.org/JPhysB/45/154016

Abstract
Femtosecond laser spectroscopies are used to investigate the influence of intramolecular nuclear modes on electronic relaxation in the cyanobacterial light harvesting protein, *C*-phycocyanin (CPC). Of particular interest are sub-ps dynamics localized on pairs of closely spaced phycocyanobilin pigments (i.e. dimers). Experiments conducted under different polarization conditions are used to distinguish isotropic and anisotropic vibrational modes within the dimers. Two isotropic nuclear modes are detected near 185 and 260 cm^{-1} using two-dimensional photon echo spectroscopy. In addition, a transient absorption anisotropy measurement reveals vibrational resonances associated with (out-of-plane) anisotropic nuclear modes near 640 and 815 cm^{-1}. We investigate two possible origins for the recurrences in the anisotropy. A mechanism involving ground state nuclear coherences in the Condon approximation is ruled out by comparing the potential energy surfaces of the excitons to the direction of wavepacket motion. Electronic structure calculations suggest that non-Condon effects are the most likely explanation for the beats observed in the anisotropy. Such non-Condon effects also hold interesting implications for the vibronic exciton electronic structure of CPC. We calculate non-Condon intermolecular couplings in the dimer as large as 10 cm^{-1}, which suggests that these effects are not negligible and deserve further consideration. Our findings provide additional insights into the sub-100 fs vibronic relaxation channel found in the closely related protein, allophycocyanin, whose pigment dimers possess nearly the same geometry and intermolecular Coulombic interactions as CPC. This study underscores the complex interplay of intramolecular vibronic coupling and site energy tuning in photosynthetic light harvesting.

(Some figures may appear in colour only in the online journal)

1. Introduction

Electronic relaxation mechanisms are currently under investigation in a wide variety of natural and artificial light harvesting antennae [1–11]. Particular interest surrounds coherent energy transfer processes, wherein electronic excitations recur at individual pigment sites within a complex before concentrating on low energy traps [2, 5]. Behind these transformative discoveries are recent advances in two-dimensional electronic spectroscopies, which enable dissection of the intermolecular couplings that control energy transfer in pigment complexes [6, 12–17]. In conjunction with experimental developments, theoretical work is leading to a clearer picture of these coherent relaxation processes [18–27]. Much of this theoretical work aims for a more realistic description of the solvent and protein bath surrounding the pigment complex.

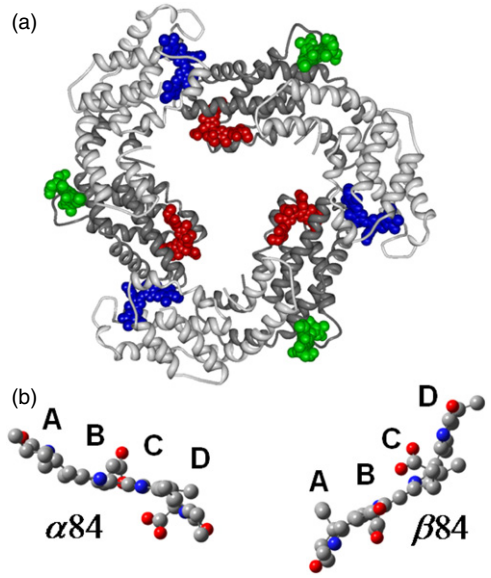

Figure 1. (a) Structure of CPC corresponding to the PDB file, 1GH0.[73] The α84 (blue) and β84 (red) phycocyanobilin pigments within the dimer possess a Coulombic coupling of approximately -150 cm^{-1}. Energy transfer processes involving the β155 phycocyanobilin pigments (green) are much slower than those occurring within the dimers. (b) The centres of mass of the α84 and β84 sites are 2 nm apart. Each pigment is an open chain tetrapyrrole in which ring A is covalently bonded to the protein through a cysteine amino acid. The HOOP vibrational modes of the phycocyanobilin pigments are localized on the methine bridges that connect the C and D pyrrole rings [58]. Adapted with permission from [30]. Copyright 2011 American Chemical Society.

By contrast, less attention has been directed towards the influence of intramolecular modes on electronic relaxation dynamics despite their clear significance in many systems. It is known, for example, that intramolecular coordinates open rapid promoting mode-assisted relaxation channels across large energy gaps in some photosynthetic complexes [28–32]. Moreover, vibronic couplings can even promote the delocalization of excited state wavefunctions between molecular sites (i.e. vibronic excitons) in acene molecular crystals [33–35], molecular aggregates [36], polypeptides [37] and light harvesting proteins [30].

In this paper, we investigate the influence of intramolecular nuclear modes on electronic relaxation in the cyanobacterial light harvesting protein, *C*-phycocyanin (CPC). The dynamics of interest are localized on the dimer units of CPC depicted in figure 1. Coulombic interactions within the dimer are much stronger than the intermolecular couplings associated with any other pair of sites in CPC [38–44]. Therefore, the fastest relaxation processes can be understood within a framework where exciton electronic states delocalize only between the α84 and β84 pigments within the dimer [30]. The most appropriate choice of basis set is not obvious in CPC because the Coulombic coupling in the dimer, which promotes exciton delocalization, is comparable to the amplitudes of the environment-induced fluctuations in the energy levels [30, 43]. As a consequence, both the Förster and modified Redfield pictures explain the $\sim$1 ps time scale of excited state population transfer reasonably well [30, 43, 45]. Recent work established the importance of a vibronic relaxation channel between exciton electronic states in a closely related cyanobacterial phycobiliprotein, allophycocyanin, whose dimer possesses a geometry and Coulombic coupling nearly identical to that in CPC [46]. Electronic population transfer is roughly ten times faster in allophycocyanin than it is in CPC despite this similar coupling strength, which points to an interplay between site energy tuning and vibronic couplings in the two proteins. We have shown that the dynamics observed in these two systems can be understood on a common footing using a vibronic exciton model [30]. CPC is further investigated here (with improved signal-to-noise ratios) to explore the possibility that inter-exciton coherences were below the detection threshold in our earlier measurements [43]. For this purpose, CPC is a more practical model than allophycocyanin because its predicted inter-exciton coherence frequencies are all less than the bandwidth of our laser. Nonetheless, insights derived from CPC will likely generalize to allophycocyanin because of their close similarities.

Vibronic exciton models are set apart from a purely electronic treatment by their inclusion of intramolecular modes in the system Hamiltonian [33]. Essentially, Franck-Condon progressions in the intramolecular modes partition the transition dipoles into a hierarchy of vibronic resonances (e.g., 0–0, 0–1 transitions known in molecular spectroscopy). The vibronic resonances located on different molecules mediate energy exchange in a manner that is analogous with more commonly employed models involving purely electronic energy gaps. Exciton delocalization naturally takes hold when the coupling between a pair of nearly degenerate vibronic levels exceeds the amplitudes of bath induced fluctuations. We examined electronic relaxation in CPC with a vibronic exciton model in [30], where an 800 cm^{-1} hydrogen out-of-plane (HOOP) wagging vibration was explicitly included in the system Hamiltonian. An energy level scheme illustrating the vibronic exciton electronic structure of CPC is shown in figure 2. In the Condon approximation, a -50 cm^{-1} vibronic coupling was computed between the 0–0 and 0–1 transition dipoles of the neighbouring α84 and β84 pigments with a reorganization energy of 100 cm^{-1} assumed for the HOOP mode. This relatively small intermolecular coupling should compete marginally against localization caused by thermal fluctuations because of their comparable magnitudes. Correlated site fluctuations are one way to sustain delocalized states in a noisy environment [47], however, we have already ruled out this possibility for CPC [48]. It is therefore of interest to examine alternative mechanisms capable of enhancing the intermolecular couplings. Non-Condon effects are potentially important in this regard because, as we show below, they can give rise to sizable transition dipole couplings without requiring unrealistically large reorganization energies in the intramolecular modes.

Our previous investigations point to the HOOP vibrations of the phycocyanobilin pigments in CPC and allophycocyanin as the key to understanding their photoinitiated dynamics. It is peculiar that these vibrations give rise to recurrences in the transient absorption anisotropies of both proteins. Vibrational beats in transient absorption anisotropies, which

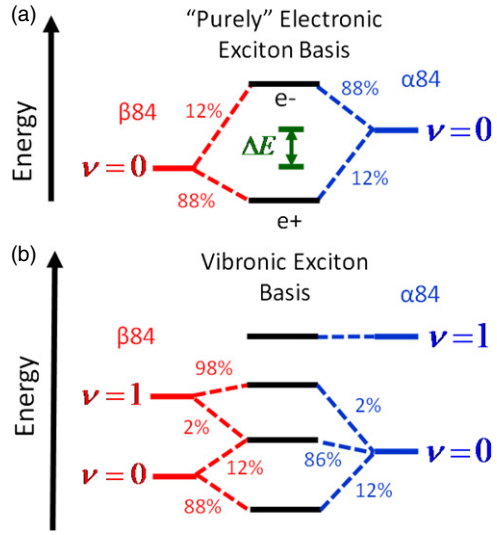

Figure 2. Electronic structures of CPC in (a) 'purely' electronic and (b) vibronic exciton models. Only the excited states of the system are shown because the Hamiltonians have block diagonal form. The difference in site energies ΔE is 350 cm^{-1} and the Coulomb coupling between transition dipoles at the electronic origin is approximately -150 cm^{-1}. Percentage contributions of the basis states (i.e. squares of the eigenvector components) to the exciton eigenvectors are taken from the calculations presented in [30]. Adapted with permission from [30]. Copyright 2011 American Chemical Society.

are fairly unusual, may offer important insights into electronic relaxation mechanisms. For example, Jonas and co-workers have investigated vibronic effects on radiative and non-radiative processes in a silicon naphthalocyanine molecule possessing D_{4h} symmetry [49–52]. In this system, the E_u excited states are doubly degenerate at the equilibrium geometry of the ground state. The excited state potentials of symmetric modes, which preserve the fourfold symmetry, are therefore displaced in the same directions with respect to the energy minimum in the ground electronic state, whereas the opposite is true for asymmetric modes. By contrast, the signs of potential energy surface displacements in the dimers of CPC cannot be predicted *a priori* based on symmetry. However, it may be that the recurrences detected in the transient absorption anisotropy of CPC originate in physics related to those at work in the silicon naphthalocyanine system. This idea was suggested to us by Jonas and co-workers in [52] and we examine this possibility here.

2. Experimental methods

CPC, isolated from *Spirulina*, was purchased from Prozyme as a suspension in 60% ammonium sulfate. Solutions of CPC were prepared in 50 mM potassium phosphate buffer at pH 7.0. All measurements were performed within 12 h of solution preparation. The solutions were circulated at a rate of 4 mL s^{-1} using a peristaltic pump with reservoir of 10 mL. The absorbance of the solution was 0.15 at 16 200 cm^{-1} with a 0.5 mm path length. Absorbance spectra were measured before and after the experiments to confirm the absence of sample degradation.

The measurements presented below were conducted under the same conditions as those employed in our earlier work [43]. For this reason, we summarize only the key aspects of the experimental methods here. Transient grating (TG) and two-dimensional photon echo (2DPE) experiments utilized an amplified Titanium Sapphire laser system producing 800 nm, 120 fs laser pulses at 1 kHz. The laser system pumped a home-built noncollinear optical parametric amplifier (NOPA) yielding 17 fs laser pulses centred at 16 000 cm^{-1} [43]. A four-wave mixing interferometer described elsewhere was used to obtain TG and 2DPE data [46]. In this setup, a diffractive optic generated a boxcars (four-pulse) laser beam geometry in which signals were detected under the phase matching condition, $\mathbf{k}_S = -\mathbf{k}_1 + \mathbf{k}_2 + \mathbf{k}_3$. Three of the incident laser pulses induced the nonlinear polarization, whereas the fourth (attenuated) pulse was used as a reference field for signal detection by spectral interferometry [53, 54]. Signals were detected with a back-illuminated CCD array (Princeton Instruments PIXIS 100B) mounted on a 0.3 m spectrograph with a 600 g mm^{-1} grating. Integration times ranged between 100–200 ms and were adjusted based on the signal intensity.

Both TG and 2DPE experiments induce the nonlinear polarization in the solution with a sequence of three laser pulses involving two experimentally controlled delays τ and T. TG measurements used a motorized translation stage to scan T (with $\tau = 0$), which is the interval in which relaxation processes such as energy transfer and solvation occur. 2DPE additionally scanned τ (at various T) by translating fused silica prism wedges in the paths of pulses 1 and 2 [55]. The delay τ is associated with absorption of the 'pump' pulses (i.e. pulses 1 and 2) and is ultimately limited by the inverse linewidth of the electronic resonance in CPC (i.e. tens of fs). Fourier transformation of the signal in τ yields the excitation dimension of the 2DPE spectrum ω_τ; the emission dimension ω_t is obtained by dispersing the signal pulse in the spectrometer.

Signal-to-noise ratios were enhanced by scanning the experimentally controlled delays multiple times and averaging. The TG experiment conducted under the magic angle polarization condition scanned the delay T ten times for a total data acquisition time of 40 min. The 2DPE experiment, which was also carried out in the magic angle configuration, required approximately 10 h because both τ and T were scanned ten times. Here the anisotropies compare tensor elements for absorptive signal components (real part of complex signal) measured in immediate succession, where data acquisition for one tensor element required approximately 35 min. This procedure yielded an error of approximately ± 0.03 in the anisotropy.

Pulses with energies of 5 nJ were focused to a 120 μm spot size at the sample for a fluence of 1.4×10^{14} photons cm^{-2}. By summing the energies of the first two pulses to arrive at the sample, we estimate that 4% of the pigments were photoexcited. This percentage corresponds to an average of 0.72 excitations per CPC hexamer. Increasing the pulse energies by a factor of four has no effect on the measured dynamics.

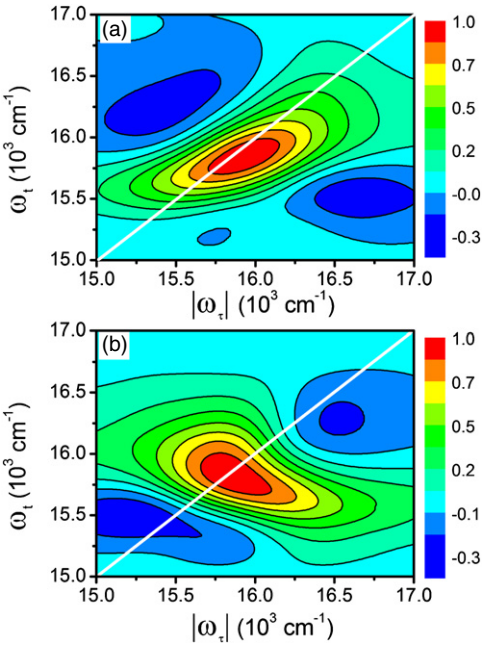

Figure 3. Real parts of (a) rephasing and (b) non-rephasing 2DPE spectra measured at $T = 0$ for CPC.

3. Results and discussion

3.1. Vibrational coherences in photon echo signals

In this section, we present 2DPE experiments conducted on CPC with the goal of detecting coherent dynamics. These new data complement our earlier work on CPC in which signatures of (incoherent) solvation processes in 2DPE signals were examined [43]. Emphasis is placed on the power spectra of the quantum beats (as opposed to the phases) because we find this representation of the signal to be most robust. Attainment of these power spectra reveals the nuclear modes associated with the largest vibronic couplings. In addition, assignments of the recurrences in the signals to vibrational motions, rather than electronic coherences, are tested by comparing rephasing and nonrephasing signal components [15]. The present experiments are carried out under the magic angle polarization condition, which is sensitive to the isotropic component of the solute response.

Experimental rephasing and non-rephasing 2DPE spectra acquired for CPC are displayed in figure 3. The line shapes of the rephasing and non-rephasing signals are respectively oriented parallel and perpendicular to the diagonals ($|\omega_\tau| = \omega_t$) of the 2D spectra. Coherent dynamics are investigated by scanning the delay between excitation and detection T and sampling the signal amplitude in a particular region of the 2D spectra. It has been shown that electronic quantum beats are best detected in the off-diagonal (diagonal) regions of the 2D spectra for the rephasing (non-rephasing) signal components [56]. By contrast, vibrational coherences can generally be measured in all regions of the rephasing and non-rephasing 2D spectra [15]. The decomposition of signal components into particular terms in the nonlinear response function is complicated by the broad line widths (>300 cm^{-1}) found in CPC at room temperature. Here, we sample areas of the

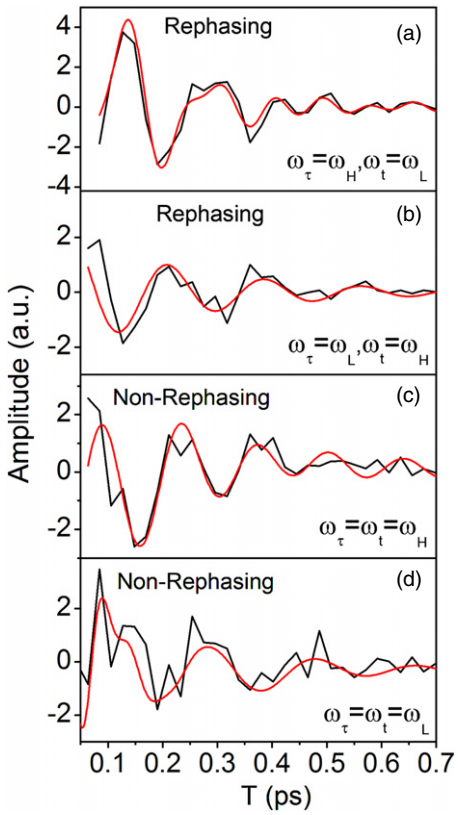

Figure 4. Real parts of (a), (b) rephasing and (c), (d) non-rephasing 2DPE signals. LPSVD fitting parameters are given in table 1. The values of the excitation ω_τ and detection ω_t frequencies are shown in the respective panels. Signal analysis is conducted with $\omega_L = 15\,900$ cm^{-1} and $\omega_H = 16\,250$ cm^{-1}.

2D spectra chosen to optimally detect electronic coherences. To this end, high and low frequency regions of the spectra are defined at $\omega_H = 16\,250$ cm^{-1} and $\omega_L = 15\,900$ cm^{-1}, respectively. The modest frequency difference $\omega_H - \omega_L$ is limited by the current signal-to-noise ratios. Still, electronic coherences should be detected, if present, because the energy gap between the single exciton states (460 cm^{-1}) is nearly resonant with $\omega_H - \omega_L$.

In figure 4, signals collected in regions of the 2DPE spectra are fit to sums of damped cosine functions

$$S(T) = \sum_{i=1} A_i \cos(\omega_i T + \phi_i) \exp(-T/\tau_i) \qquad (1)$$

for which the fitting parameters are given in table 1. The fits reveal recurrences corresponding to two vibrational modes. The lower frequency resonance is detected in the 175–193 cm^{-1} range. Although the fitting parameters vary, we suggest that recurrences in this spectral range most likely represent a common nuclear coordinate because the relatively short damping time constants (<0.33 ps) give rise to line widths that are broader than the 18 cm^{-1} range in the central frequency (cf, figure 5). It is possible that inhomogeneous broadening is responsible for these relatively fast damping rates. Higher frequency resonances are found in the 246–274 cm^{-1} spectral region. Again, we assign recurrences in this range to a common vibrational coordinate because the line widths are broader than the 28 cm^{-1} range in the

Table 1. LPSVD fitting parameters for PE signals.

Parameter[a,b]	Rephasing $\omega_\tau = \omega_H, \omega_t = \omega_L$	Rephasing $\omega_\tau = \omega_L, \omega_t = \omega_H$	Non-rephasing $\omega_\tau = \omega_t = \omega_H$	Non-rephasing $\omega_\tau = \omega_t = \omega_L$
A_1	1.0	0.34	0.41	0.38
ω_1 (cm^{-1})	193	188	175	176
ϕ_1 (rad)	0.18	0.52	1.02	1.10
τ_1 (ps)	0.12	0.24	0.33	0.24
A_2	0.23	–	0.56	–
ω_2 (cm^{-1})	274	–	246	–
ϕ_2 (rad)	1.10	–	0.05	–
τ_2 (ps)	0.21	–	0.67	–

[a] In the experiments, $\omega_L = 15\,900$ cm^{-1} and $\omega_H = 16\,250$ cm^{-1}.
[b] Only LPSVD components with amplitudes that are at least 5% of the maximum amplitude found in the fit are given.

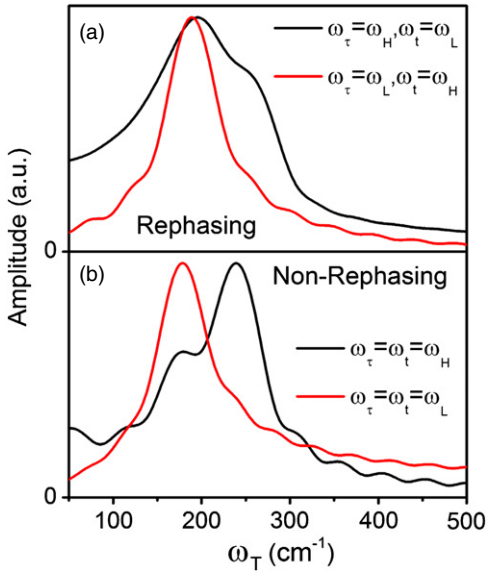

Figure 5. Plots of the (a) rephasing and (b) non-rephasing LPSVD fitting components given in table 1. The corresponding time domain signals are shown in figure 4.

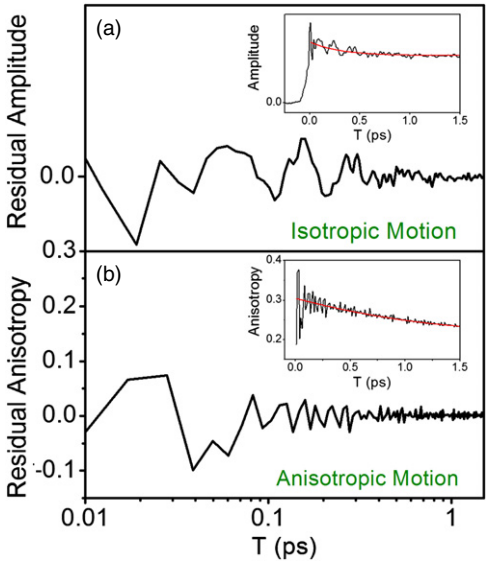

Figure 6. (a) TG signals acquired under the magic angle polarization condition are sensitive to isotropic nuclear motion. (b) Vibrational coherences in the transient absorption anisotropy are associated with anisotropic nuclear motion. The insets show how the vibrational coherences are isolated by subtracting decaying exponentials from the measured signals.

central frequency. It is interesting that the higher frequency mode is found only with the higher excitation frequency $\omega_\tau = \omega_H$. We hypothesize that photoexcitation further above the purely electronic transition frequency (i.e. $\omega_\tau = \omega_H$ versus $\omega_\tau = \omega_L$) more readily initiates wavepacket motion in the 246–274 cm^{-1} range. The effect is understood by considering that, for resonant terms, the mode frequency equates to the difference in the frequency components associated with the first two field-matter interactions. Thus, nonlinearities in which the system first interacts with a higher frequency component of the laser are enhanced because the zero quantum vibrational levels of the 246–274 cm^{-1} modes are primarily populated at equilibrium ($k_BT \approx 200$ cm^{-1}). Finally, we note that all of the observed recurrences are assigned to vibrational motion because they are detected in both rephasing and non-rephasing 2D spectra [15].

3.2. Distinguishing isotropic and anisotropic motion with electric field polarizations

The 2DPE measurements presented above are sensitive to isotropic motion because the magic angle polarization condition is employed. The anisotropic modes, which have periods that challenge our 20 fs time resolution, are best studied with TG (rather than 2DPE) because its shorter data acquisition time facilitates signal averaging. The tradeoff for the improved signal-to-noise ratio obtained in TG is the loss of resolution in the excitation dimension ω_τ. Nonetheless, the information provided by TG is useful for establishing basic insights into the influence of intramolecular modes on the electronic population transfer process.

First, we present TG signals obtained under the magic angle polarization condition. Figure 6 shows that the incoherent part of the TG signal associated with electronic populations must first be subtracted to isolate the coherent nuclear dynamics of interest. The residual signal amplitude is then Fourier transformed to obtain the vibrational spectrum shown in figure 7. A direct Fourier transformation is employed because we find this to be more reliable than the LPSVD fitting algorithm for these data, which contain several oscillatory components. The isotropic spectrum is dominated by a peak

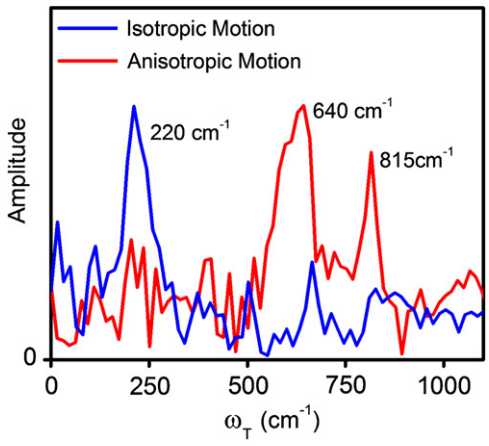

Figure 7. Fourier transformation of the residual in the TG signal amplitude (blue) yields the spectrum of isotropic nuclear motion. The spectrum of anisotropic nuclear motion is obtained by Fourier transforming the residual of the transient absorption anisotropy. The residuals used to generate these spectra are shown in figure 6.

near 220 cm^{-1}. It is likely that this peak has contributions from the two vibrational modes detected in the 2DPE experiments above. Additional resonances may be present near 500 and 660 cm^{-1}. However, definitive assignments cannot be made with the current signal-to-noise ratio.

Anisotropic vibrational modes are detected by carrying out a similar analysis on the absorptive part of the TG anisotropy. The real (absorptive) parts of the measured TG signals $S_{\parallel}(T)$ and $S_{\perp}(T)$ are used to generate the anisotropy $r(T)$ using

$$r(T) = \frac{S_{\parallel}(T) - S_{\perp}(T)}{S_{\parallel}(T) + 2S_{\perp}(T)}. \tag{2}$$

In this notation, the $S_{\parallel}(T)$ tensor element involves all-parallel electric field polarizations, whereas in $S_{\perp}(T)$ pulses 1 and 2 have polarizations orthogonal to pulse 3 and the signal. We remark that the magic angle polarization condition yields the linear combination of tensor elements shown in the denominator of equation (2). In figure 6(b), an exponential decay is subtracted from $r(T)$ to isolate the coherent part of the response. The Fourier transform of the residual is overlaid with the spectrum corresponding to the isotropic response in figure 7. This comparison shows that the two classes of nuclear motions are readily distinguished in the isotropic and anisotropic TG signals. The spectrum of anisotropic motion possesses two resonances at 640 and 815 cm^{-1}. Our earlier experiments were only able to resolve a single resonance in this frequency region, which was assigned to a HOOP vibrational mode [43]. The present measurement is consistent with earlier resonance Raman studies of isotopic derivatives in which multiple vibrations near 800 cm^{-1} were found to possess out-of-plane character [57–59].

3.3. Influence of ground state wavepacket motion on the transient absorption anisotropy

In this section, we consider the possibility that motion of a ground state wavepacket brings the system into regions of coordinate space which carry different sensitivities to resonances with particular excitons, thereby varying the angle of the signal field polarization. Signs of the displacements in excited state potential energy surfaces are the key quantities underlying vibrational modulation of the transient absorption anisotropy in some systems [50, 52]. A qualitative picture is sufficient for establishing the basic physics. In this view of CPC, all nuclear modes are regarded as part of the bath and the system is 'purely' electronic (cf, figure 2(a)). As in [30], the Frenkel exciton Hamiltonian of the dimer can then be written as [24, 60]

$$H_{\mathrm{Sys}}^{\mathrm{el}} = \sum_{m=1}^{2} E_m B_m^{\dagger} B_m + \sum_{m=1}^{2}\sum_{n\neq m}^{2} J_{mn} B_m^{\dagger} B_n, \tag{3}$$

where the basis is composed of purely electronic two-level systems. E_m is the thermally averaged energy gap of pigment m at the ground state equilibrium geometry (i.e. Franck–Condon geometry) and J_{mn} is the Coulombic coupling between molecules m and n. Interactions between the system and bath enter this reduced description by way of correlation functions [61]. Low frequency motion of the solvent and protein cause thermal fluctuations in E_m, which reflect the exchange of vibrational quanta between the system and bath. By contrast, higher frequency intramolecular modes give rise to Franck-Condon progressions in optical spectra and potentially open efficient relaxation channels across energy gaps that are much larger than $k_B T$. The 800 cm^{-1} HOOP vibration can be treated as underdamped harmonic modes whose spectral density is given by [61]

$$C_m^{\mathrm{HOOP}}(\omega) = \tfrac{1}{2} d_m^2 \Omega_m^2 \left[\delta(\omega - \omega_m) - \delta(\omega + \omega_m)\right]. \tag{4}$$

Here d_m and $\frac{1}{2} d_m^2 \omega_m$ are respectively the dimensionless potential energy surface displacement and reorganization energy for the HOOP mode at site m. Assuming that each site in the dimer possesses an uncorrelated bath, the local spectral densities of the HOOP modes are transformed into the single exciton basis using

$$C_{ab}^{\mathrm{HOOP}}(\omega) = \sum_{m=1}^{2} \phi_{am}^2 \phi_{bm}^2 C_m^{\mathrm{HOOP}}(\omega), \tag{5}$$

where the eigenvector of exciton a is written as

$$|a\rangle = \sum_{m=1}^{2} \phi_{am} |m\rangle. \tag{6}$$

We focus only on the component of the spectral density involving the HOOP vibration because the physics of interest can be understood without treating lower frequency thermal motion in the bath.

Insights into the impact of the HOOP mode on the anisotropy are obtained by visualization of the potential energy surfaces. For illustration, we assume that the HOOP vibrational frequencies ω_m and the displacements d_m are equivalent at the two sites. For convenience, the local spectral densities $C_1^{\mathrm{HOOP}}(\omega)$ and $C_2^{\mathrm{HOOP}}(\omega)$ will hereafter be written as $C_{\mathrm{local}}^{\mathrm{HOOP}}(\omega)$. The potential energy surfaces associated with the local basis is presented in figure 8(a). The HOOP vibration at site m is displaced only when site m is photoexcited. In the opposite limit, we have the spectral densities of a homodimer (where $E_1 = E_2$), which for excitons e+ and e− reads as

$$C_{++}^{\mathrm{HOOP}}(\omega) = C_{--}^{\mathrm{HOOP}}(\omega) = \tfrac{1}{2} C_{\mathrm{local}}^{\mathrm{HOOP}}(\omega). \tag{7}$$

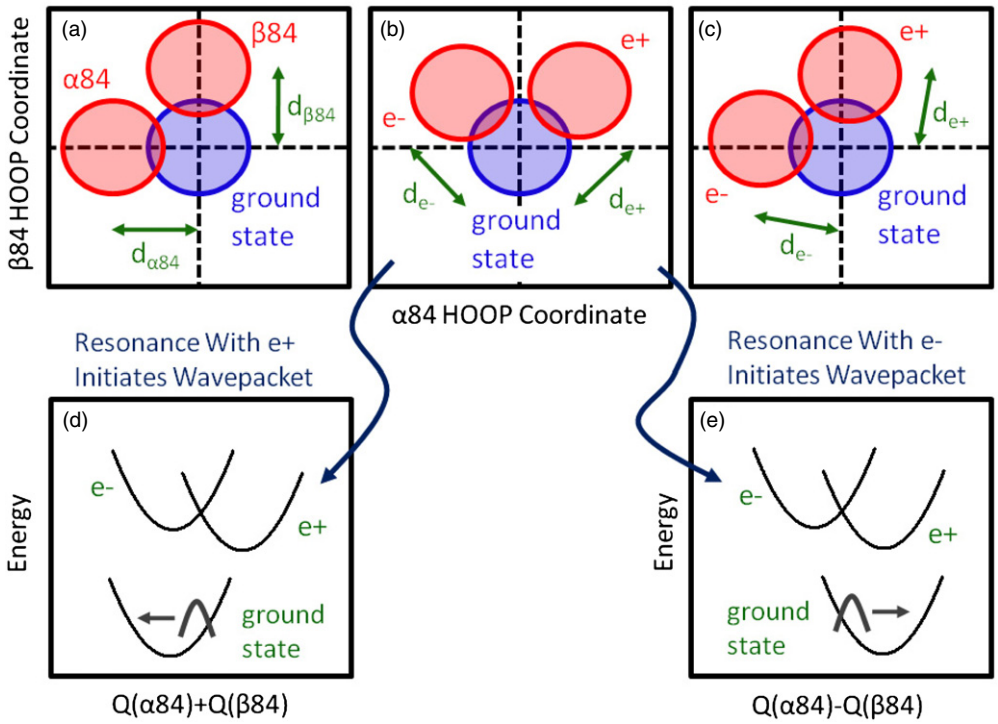

Figure 8. Harmonic ground (blue) and excited state (red) potential energy wells of the HOOP modes are shown in the top row. (a) In the local basis, the two pigments do not possess shared modes. Excitation of pigment $\alpha 84$ ($\beta 84$) displaces only the HOOP mode for site $\alpha 84$ ($\beta 84$). (b) The HOOP coordinates contribute equally to the spectral densities of the e+ and e− exciton states in a homodimer. The resonance with e+ (e−) initiates ground state wavepacket motion parallel to the displacement, d_{e+} (d_{e-}). (c) The HOOP coordinates do not contribute equally to the spectral densities of the e+ and e− exciton states in a heterodimer. Still, the ground state wavepacket driven by the resonance with e+ (e−) travels parallel to the displacement d_{e+} (d_{e-}). (d) Slice taken (diagonally) through the surfaces in panel (b). (e) Anti-diagonal slice taken from the potential energy surfaces in panel (b).

The coefficient of $1/2$ says that the potential energy surface displacements of the excitons are smaller than those found in the individual pigments (i.e. exchange narrowing). As shown in figure 8(b), both local HOOP coordinates are equally displaced by excitation of either of the two exciton states in a homodimer. The picture relevant for a heterodimer, such as CPC, is shown in figure 8(c); exchange narrowing is suppressed and the orientations of the surface displacements become more like those found in the local basis. For example, if $|E_1 - E_2| \gg J_{12}$, then the spectral densities of the excitons can be approximated as

$$C_{++}^{\mathrm{HOOP}}(\omega) = C_{--}^{\mathrm{HOOP}}(\omega) \approx C_{\mathrm{local}}^{\mathrm{HOOP}}(\omega). \tag{8}$$

The important point is that, in both the homodimer and heterodimer, photoexcitation initiates ground state wavepacket motion in a direction that is parallel to the potential energy surface displacement for one exciton and orthogonal to the other. Slices cut along the two directions of wavepacket motion are shown in figure 8. Notably, the two surfaces are not displaced in opposite directions with respect to the ground state minimum as in the silicon naphthalocyanine system [52]. Therefore, these potential energy surfaces predict vibrational coherences in the individual tensor elements $S_{\parallel}(T)$ and $S_{\perp}(T)$, but not in the anisotropy $r(T)$. We have confirmed that the qualitative and intuitive picture presented in figure 8 is consistent with numerical calculations employing a rigorous response function formalism [24].

The above discussion assumes that the $\alpha 84$ and $\beta 84$ HOOP vibrational modes are not delocalized between pigments. Such delocalization would change the physics entirely because each of the local spectral densities $C_m^{\mathrm{HOOP}}(\omega)$ would then possess contributions from nuclear modes delocalized between sites. Through-space Coulombic coupling can promote the delocalization of vibrational modes in the absence of covalent bonds [62]. However, we rule out this possibility for the HOOP modes in the dimer of CPC because of the large distance (>2 nm) between modes.

3.4. Non-Condon character of the HOOP vibrational mode

Implicit in section 3.3 is the assumption that the electronic transition dipoles are independent of nuclear coordinates. In this section, we look beyond this approximation because non-Condon effects are a second way that the HOOP mode can couple to the polarization of the TG signal field. Condon and non-Condon terms are defined by carrying out an expansion on a transition dipole matrix element connecting two vibronic quantum states [63]

$$\langle 0|\langle g|\vec{\mu}|e\rangle|\nu\rangle = \vec{\mu}_{\mathrm{ge}}^{\mathrm{el}}\langle 0\mid\nu\rangle + \left(\frac{\partial\vec{\mu}_{\mathrm{ge}}^{\mathrm{el}}}{\partial Q}\right)_{Q_0}\langle 0|Q|\nu\rangle + \cdots. \tag{9}$$

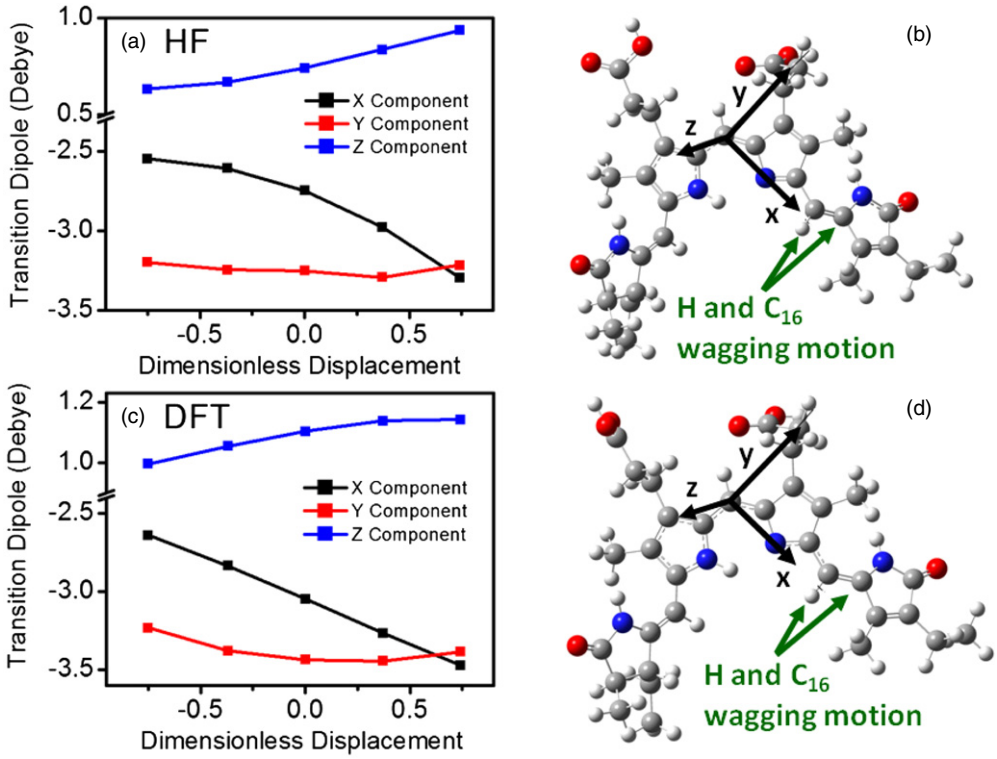

Figure 9. Shown on the left are transition dipole components computed at the (a) HF/6–311G(d) and (c) B3LYP/6–311G(d) levels of theory. The Cartesian coordinate systems and ground state equilibrium geometries associated with the HF/6–311G(d) and B3LYP/6–311G(d) models are presented in panels (b) and (d), respectively. Dimensionless displacements in the HOOP coordinates are generated by scaling the normal modes with a factor of $\sqrt{m\omega/\hbar}$, where m is the reduced mass and ω is the vibrational frequency. For both models, vibrational motion primarily involves anti-correlated out-of-plane motion of the indicated H and C_{16} atoms.

Here $\vec{\mu}_{ge}^{el}$ is the 'purely' electronic transition dipole connecting the ground state g and the excited electronic state e; $\langle 0 \mid \nu \rangle$ is a vibrational overlap integral (whose square is a 'Franck–Condon factor'); $\langle 0 | Q | \nu \rangle$ is a vibrational matrix element that peaks near $\nu = 1$ when the reorganization energy for mode Q is small (in which case it parallels selection rules in infrared spectroscopy). Equation (9) assumes that the transition initiates at the zero quantum vibrational level of the ground electronic state and terminates in level ν of the excited state e. The expansion is truncated at the leading term in the Condon approximation under the assumption that the derivative of the dipole in the second term is small.

With respect to the transient absorption anisotropy, the key question is whether or not motion along the HOOP coordinates affects the magnitudes and orientations of the site transition dipoles in CPC. Such coupling of the transition dipole to the geometry will be reflected in the signal field polarization. To address this possibility, we use electronic structure models (implemented in Gaussian 2009 [64]) to compute electronic transition dipoles at various displacements in the HOOP coordinate for an individual phycocyanobilin pigment. The calculations are carried out in a dielectric environment (dielectric constant equal to 4.0 in the 'polarizable continuum model' [64]) to simulate the surrounding protein environment [65, 66]. Because the 'best' choice of an electronic structure method is not clear *a priori*, we employ two different models to ensure robust insights: (i) B3LYP functional with 6–311G(d) basis set; (ii) Hartree–Fock with 6–311G(d) basis set. Figure 9 shows that the two levels of theory yield similar ground state geometries and normal modes. The HOOP modes are computed at 678 cm^{-1} and 733 cm^{-1} in the B3LYP and Hartree–Fock models, respectively. Assignments of the HOOP modes are based on the vibrational frequency and out-of-plane motion localized on the methine bridge linking pyrrole rings C and D [58]. Although this mode is nominally characterized by out-of-plane motion of the hydrogen atom on the methine bridge, we note that the calculations also predict substantial amplitude on the carbon atom to which the hydrogen atom is bonded and its neighbour located in ring D (i.e. C_{15} and C_{16} in [58]). At both levels of theory, the hydrogen atom and C_{16} exhibit anti-correlated out-of-plane motion; C_{16} is closer to being in-plane when H is out-of-plane and vice versa.

We next compute transition dipoles for the $\pi\pi^*$ excitation (HOMO to LUMO transition) at various positions along the HOOP coordinates. The calculated dipoles are plotted with respect to the dimensionless excited state displacement in the HOOP mode in figure 9, where the dimensionless coordinate is obtained by multiplying the normal mode by $\sqrt{m\omega/\hbar}$ (m is the reduced mass and ω is the mode frequency) [61]. Displacement in the positive direction brings the H atom closer to being 'in-plane' and the C_{16} atom 'out-of-plane' (towards positive z in the Cartesian coordinate system shown in figure 9); the opposite is true for negative displacements. At both levels of theory, the x and z components of the dipoles respectively increase and decrease with positive displacements, whereas the y components of the dipoles are less sensitive to changes

in the geometry. We take this qualitative agreement between the models as an indication that the physical insights are robust. Based on these calculations, we hypothesize that non-Condon effects are at the root of the recurrences observed in the transient absorption anisotropy. This explanation is most likely considering that both electronic coherences and the mechanism in section 3.3 have already been ruled out.

3.5. Impact of non-Condon effects on vibronic exciton electronic structure

It is of interest to consider the impact of non-Condon terms on the intermolecular couplings underlying the vibronic exciton electronic structure shown in figure 2(b). The physics are made clear by writing the vibronic exciton Hamiltonian [30]

$$H_{\mathrm{Sys}}^{\mathrm{vb}} = \sum_{m=1}^{2}\sum_{\nu=0}\left(E_m + \nu\hbar\omega_\nu\right) B_{m\nu}^{\dagger} B_{m\nu} + \sum_{m=1}^{2}\sum_{n\neq m}^{2}\sum_{\nu=0}\sum_{\sigma=0} V_{m\nu,n\sigma} B_{m\nu}^{\dagger} B_{n\sigma}. \tag{10}$$

The indices m and n represent molecular sites, ν and σ are vibronic levels at sites m and n, and ω_ν is the frequency of the HOOP intramolecular mode. In this notation, the operator $B_{m\nu}^{\dagger}$ ($B_{m\nu}$) creates (annihilates) an excitation at molecule m in vibronic level ν. The single exciton block of the Hamiltonian matrix is constructed in a basis of vibronic excitations denoted as $|m, \nu\rangle$, which upon diagonalization yields

$$|a\rangle = \sum_{m=1}^{2}\sum_{\nu=0}\phi_{a,m\nu}\,|m, \nu\rangle. \tag{11}$$

When the lowest order non-Condon term is considered, the Coulombic coupling expands into a hierarchy of interactions

$$V_{m\nu,n\sigma} = J_{mn}\,\langle 0 \mid \nu\rangle\,\langle 0 \mid \sigma\rangle + K_{mn}\,\langle 0 \mid \nu\rangle\,\langle 0|\,Q\,|\sigma\rangle + K_{nm}\,\langle 0 \mid \sigma\rangle\,\langle 0|\,Q\,|\nu\rangle + L_{nm}\,\langle 0|\,Q\,|\nu\rangle\,\langle 0|\,Q|\sigma\rangle. \tag{12}$$

The usual (Condon) transition dipole coupling is given by

$$J_{mn} = \frac{\vec{\mu}_m^{\mathrm{el}}\cdot\vec{\mu}_n^{\mathrm{el}} - 3\left(\vec{\mu}_m^{\mathrm{el}}\cdot\hat{n}_{mn}\right)\left(\vec{\mu}_n^{\mathrm{el}}\cdot\hat{n}_{mn}\right)}{4\pi\,\varepsilon_0 R_{mn}^3}, \tag{13}$$

where $\vec{\mu}_m^{\mathrm{el}}$ is the purely electronic transition dipole for the electronic resonance at site m. The higher order non-Condon coefficients are

$$K_{mn} = \frac{\vec{\mu}_m^{\mathrm{el}}\cdot\left(\frac{\partial\vec{\mu}_n^{\mathrm{el}}}{\partial Q}\right)_{Q_0} - 3\left(\vec{\mu}_m^{\mathrm{el}}\cdot\hat{n}_{mn}\right)\left(\left(\frac{\partial\vec{\mu}_n^{\mathrm{el}}}{\partial Q}\right)_{Q_0}\cdot\hat{n}_{mn}\right)}{4\pi\,\varepsilon_0 R_{mn}^3}, \tag{14}$$

$$L_{mn} = \frac{\left(\frac{\partial\vec{\mu}_m^{\mathrm{el}}}{\partial Q}\right)\cdot\left(\frac{\partial\vec{\mu}_n^{\mathrm{el}}}{\partial Q}\right)_{Q_0} - 3\left(\left(\frac{\partial\vec{\mu}_m^{\mathrm{el}}}{\partial Q}\right)\cdot\hat{n}_{mn}\right)\left(\left(\frac{\partial\vec{\mu}_n^{\mathrm{el}}}{\partial Q}\right)_{Q_0}\cdot\hat{n}_{mn}\right)}{4\pi\,\varepsilon_0 R_{mn}^3}. \tag{15}$$

We remark that J_{mn} and K_{mn} are reminiscent of Albrecht's A and B terms for Raman scattering [67].

In the Condon approximation, the product of overlap integrals between nuclear wavefunctions $\langle 0 \mid \nu\rangle\ \langle 0 \mid \sigma\rangle$ distributes the inter-site Coulombic coupling J_{mn} in the vibronic basis. These overlap integrals make the Condon couplings quite sensitive to the mode displacements (i.e. reorganization energies). The terms K_{mn} and K_{nm} incorporate couplings between the purely electronic transition dipole at one site and the dipole derivative at a second site. Finally, the L_{mn} term involves intermolecular interactions between pairs of dipole derivatives. The relative weights of these terms can be estimated using the electronic structure models introduced in the previous section. Much of the necessary information can be obtained directly from the results shown in figure 9 (e.g., transition dipole derivatives). Because the site transition dipoles are calculated for equilibrium structures generated by model calculations, the dipole orientations in the dimer are configured by assuming an angle of 60° between the dipoles at the α84 and β84 sites [43]. The HOOP mode displacements needed to evaluate the integrals $\langle 0 \mid \nu\rangle$ and $\langle 0|\,Q\,|\nu\rangle$ are computed by transforming the Cartesian excited state gradients onto the normal coordinate and further assuming that the mode is harmonic and possesses equal ground and excited state frequencies [68]. These mode displacements are taken to be equivalent for both sites. Finally, the transition dipoles and their derivates are linearly scaled by factors of 2.5 and 2.7 for the B3LYP and Hartree–Fock models to generate intermolecular couplings in the range known for CPC [30]. These scaled transition dipole sizes are consistent with those found in other bilin pigments [69–71].

Terms computed at both levels of theory are summarized in table 2. The calculations are restricted to the pairs of levels between which delocalization is indicated in figure 2 because interactions between higher-lying vibronic levels are negligible. Inspection of the calculated couplings suggests that, with the exception of $K_{12}\,\langle 0 \mid 0\rangle\,\langle 0|\,Q\,|1\rangle$, the non-Condon terms are generally small and can probably be neglected. The $K_{12}\,\langle 0 \mid 0\rangle\,\langle 0|\,Q\,|1\rangle$ term is particularly interesting because vibronic interactions between this pair of levels is the key to the different behaviours found in CPC and allophycocyanin [30]. As illustrated in figure 2, the '0–1' resonance at the β84 pigment couples with the '0–0' resonance at α84 in the vibronic exciton Hamiltonian. Little delocalization is found in CPC because of the 450 cm^{-1} difference in the resonance frequencies. By contrast, the key to the fast dynamics observed in allophycocyanin is that the difference in resonance frequencies is less than 50 cm^{-1} [31]. Our model calculations suggest that the calculated Condon and non-Condon terms $J_{12}\,\langle 0 \mid 1\rangle\,\langle 0 \mid 0\rangle$ and $K_{12}\,\langle 0 \mid 0\rangle\,\langle 0|\,Q\,|1\rangle$ differ by less than a factor of 3. Of course, these couplings are sensitive to the sizes of the calculated displacements, which are smaller than we had expected (particularly for the B3LYP/6–311G(d) model). Indeed, large resonance Raman cross sections [58] and the vibronic modulations in our TG signals are difficult to justify for a dimensionless displacement of 0.1. In table 2, we re-calculate the couplings using the B3LYP/6–311G(d) model with an *ad hoc* displacement of 0.4. The $-50\ \mathrm{cm}^{-1}$ coupling found by adding the $J_{12}\,\langle 0 \mid 1\rangle\,\langle 0 \mid 0\rangle$ and $K_{12}\,\langle 0 \mid 0\rangle\,\langle 0|\,Q\,|1\rangle$ terms together is equivalent to that

Table 2. Calculated intermolecular couplings.

Parameter[a]	HF/6–311G(d)	B3LYP/6–311G(d)	B3LYP/6–311G(d)[b]
d	0.26	0.10	0.40
$J_{12}\langle 0 \mid 0\rangle\langle 0 \mid 0\rangle$	-144.9 cm^{-1}	-149.2 cm^{-1}	-138.4 cm^{-1}
$J_{12}\langle 0 \mid 1\rangle\langle 0 \mid 0\rangle$	-26.6 cm^{-1}	-10.5 cm^{-1}	-39.1 cm^{-1}
$K_{12}\langle 0 \mid 0\rangle\langle 0\mid Q\mid 0\rangle$	1.8 cm^{-1}	0.7 cm^{-1}	2.7 cm^{-1}
$K_{12}\langle 0 \mid 0\rangle\langle 0\mid Q\mid 1\rangle$	-10.2 cm^{-1}	-10.5 cm^{-1}	-10.5 cm^{-1}
$K_{12}\langle 0 \mid 1\rangle\langle 0\mid Q\mid 0\rangle$	-1.9 cm^{-1}	-0.7 cm^{-1}	-3.0 cm^{-1}
$L_{12}\langle 0\mid Q\mid 0\rangle\langle 0\mid Q\mid 0\rangle$	0.0 cm^{-1}	0.0 cm^{-1}	-0.1 cm^{-1}
$L_{12}\langle 0\mid Q\mid 0\rangle\langle 0\mid Q\mid 1\rangle$	0.1 cm^{-1}	0.1 cm^{-1}	0.2 cm^{-1}

[a] A distance between dipoles R_{12} of 2 nm is assumed.
[b] The dimensionless displacement d is set equal to 0.4 for illustration. All other parameters are obtained using the B3LYP/6–311G(d) model.

computed in [30] but employs a reorganization energy that is 36% smaller. Because there is currently some uncertainty in the size of the displacement, we reach the conservative conclusion that non-Condon contributions to the intermolecular vibronic couplings in CPC probably exceed 20%.

4. Conclusion

In conclusion, femtosecond laser spectroscopies have been used to investigate the influence of intramolecular nuclear motions on electronic relaxation within the pigment dimers of CPC. 2DPE experiments conducted under the magic angle polarization condition reveal two isotropic nuclear modes near 185 and 260 cm^{-1}. TG experiments also detect vibrational amplitude in this same spectral region. In addition, vibrational resonances associated with anisotropic nuclear modes are found at 640 and 815 cm^{-1} in the transient absorption anisotropy. The 815 cm^{-1} resonance is assigned to HOOP-like motion on the methine bridge linking pyrrole rings C and D (cf, figure 1). Two mechanisms that potentially give rise to recurrences in the transient absorption anisotropy are examined. First, with inspiration taken from recent work on a silicon naphthalocyanine system [50–52], we consider the role of ground state wavepacket motion in the Condon approximation. Contributions from this mechanism are ruled out by comparing the potential energy surfaces of the excitons to the directions of wavepacket motion (cf, figure 8). The possibility that non-Condon effects influence the optical response is also investigated with electronic structure calculations. It is found that both the transition dipole magnitude and orientation vary significantly for small (realistic) displacements along the HOOP coordinate (cf, figure 9). Based on these calculations, we believe it is most likely that non-Condon effects are at the origin of the recurrences observed in the anisotropy. This hypothesis can be experimentally tested by conducting anisotropy measurements on the sub-units of CPC possessing single phycocyanobilin pigments.

We have shown that non-Condon effects have important implications for the vibronic exciton electronic structure of CPC (and allophycocyanin). Equation (12) describes how the Coulombic intermolecular coupling partitions into a hierarchy of terms when non-Condon effects are taken into account. It is interesting to consider the possibility that the intermolecular vibronic interactions in CPC are enhanced by the higher order terms. With such enhancements, the delocalization of vibronic states in CPC would not require such a large (and unrealistic?) reorganization energy in the HOOP mode. For example, in the notation of equation (12), we compute a coupling $V_{10,11}$ of approximately -50 cm^{-1} for CPC in the Condon approximation when the reorganization energy in the HOOP mode is 100 cm^{-1} [30]. By contrast, it is shown in table 2 that a coupling of -50 cm^{-1} is obtained with a reorganization energy of 64 cm^{-1} when non-Condon effects are included. Quantitative conclusions regarding the influence of non-Condon effects on the electronic structure cannot be drawn at this point and further investigation is needed. Resonance Raman experiments will be useful for determining the size of the displacement in the HOOP mode. Future work should also consider the influence of Duchinsky rotation on the intermolecular couplings [72].

The relatively slow relaxation process in CPC contrasts markedly with the sub-100 fs dynamics found in the closely related protein, allophycocyanin, whose pigment dimers have nearly the same geometry and intermolecular Coulombic coupling [31, 73, 74]. The main differences between the dimers in these two proteins are the energy gaps at the individual pigment sites. In allophycocyanin, the difference in site energies is nearly resonant with the 800 cm^{-1} HOOP mode [30, 31]. Therefore, vibronic exciton wavefunctions more readily delocalize in this system than in CPC. It was suggested by Beck and co-workers that allophycocyanin may have evolved such a fast relaxation process in order to trap the electronic excitation on the lower energy $e+$ exciton level [74]. The key idea is that the release of heat accompanying the $e- \rightarrow e+$ transition helps to ensure that energy transfer within the phycobilisome is unidirectional because the 800 cm^{-1} gap between excited states is much larger than k_BT.

Acknowledgments

This material is based upon work supported by the National Science Foundation under CHE-0952439. We thank the reviewers for helpful suggestions. JMW and BAW acknowledge the Institute for the Environment at the University of North Carolina for graduate fellowships. NFS thanks the NSF (CHE-1059057) for financial support.

References

[1] Calhoun T R, Ginsberg N S, Schlau-Cohen G S, Cheng Y C, Ballottari M, Bassi R and Fleming G R 2009 *J. Phys. Chem.* B **113** 16291–5

[2] Collini E, Wong C Y, Wilk K E, Curmi P M G, Brumer P and Scholes G D 2010 *Nature* **463** 644–7

[3] Womick J M, Miller S A and Moran A M 2009 *J. Phys. Chem.* A **113** 6587–98

[4] Panitchayangkoon G, Hayes D, Fransted K A, Caram J R, Harel E, Wen J, Blankenship R E and Engel G S 2010 *Proc. Natl Acad. Sci.* **107** 12766–70

[5] Engel G S, Calhoun T R, Read E L, Ahn T K, Mancal T, Cheng Y C, Blankenship R E and Fleming G R 2007 *Nature* **446** 782–6

[6] Myers J A, Lewis K L M, Fuller F D, Tekavec P F, Yocum C F and Ogilvie J P 2010 *J. Phys. Chem. Lett.* **1** 2774–80

[7] Zhu J, Gdor I, Smolensky E, Friedman N, Sheves M and Ruhman S 2010 *J. Phys. Chem.* B **114** 3038–45

[8] Sperling J, Nemeth A, Hauer J, Abramavicius D, Mukamel S, Kauffmann H F and Milota F 2010 *J. Phys. Chem.* A **114** 8179–89

[9] Feng X, Neupane B, Acharya K, Zazubovich V, Picorel R, Seibert M and Jankowiak R 2011 *J. Phys. Chem.* B **115** 13339–49

[10] Abramavicius D, Nemeth A, Milota F, Sperling J, Mukamel S and Kauffmann H F 2012 *Phys. Rev. Lett.* **108** 067401

[11] Bixner O *et al* 2012 *J. Chem. Phys.* **136** 204503

[12] Jonas D M 2003 *Annu. Rev. Phys. Chem.* **54** 425–63

[13] Cowan M L, Ogilvie J P and Miller R J D 2004 *Chem. Phys. Lett.* **386** 184–9

[14] Tian P, Keusters D, Suzaki Y and Warren W S 2003 *Science* **300** 1553–5

[15] Turner D B, Stone K W, Gundogdu K and Nelson K A 2011 *Rev. Sci. Instrum.* **82** 081301

[16] Turner D B, Wilk K E, Curmi P M G and Scholes G D 2011 *J. Phys. Chem. Lett.* **2** 1904–11

[17] Lott G A, Perdomo-Ortiz A, Utterback J K, Widom J R, Aspuru-Guzik A and Marcus A H 2011 *Proc. Natl Acad. Sci.* **108** 16521–6

[18] Hennebicq E, Beljonne D, Curutchet C, Scholes G D and Silbey R J 2009 *J. Chem. Phys.* **130** 214505

[19] Nazir A 2009 *Phys. Rev. Lett.* **103** 146404

[20] Fassioli F, Nazir A and Olaya-Castro A 2010 *J. Phys. Chem. Lett.* **1** 2139–43

[21] Chin A W, Datta A, Caruso F, Huelga S F and Plenio M B 2010 *New J. Phys.* **12** 065002

[22] Yuen-Zhou J, Krich J J, Mohseni M and Aspuru-Guzik A 2011 *Proc. Natl Acad. Sci* **108** 17615–20

[23] Sarovar M, Ishizaki A, Fleming G R and Whaley K B 2010 *Nature Phys.* **6** 462–7

[24] Abramavicius D, Palmieri B, Voronine D V, Sanda F and Mukamel S 2009 *Chem. Rev.* **109** 2350–408

[25] Ishizaki A and Fleming G R 2009 *Proc. Natl Acad. Sci.* **106** 17255–60

[26] Olbrich C, Strümpfer J, Schulten K and Kleinekathoefer U 2011 *J. Phys. Chem.* B **115** 758–64

[27] Plenio M B and Huelga S F 2008 *New J. Phys.* **10** 113019

[28] Arnett D C, Moser C C, Dutton P L and Scherer N F 1999 *J. Phys. Chem.* B **103** 2014–32

[29] Jonas D M, Lang M J, Nagasawa Y, Joo T and Fleming G R 1996 *J. Phys. Chem* **100** 12660–73

[30] Womick J M and Moran A M 2011 *J. Phys. Chem.* B **115** 1347–56

[31] Womick J M and Moran A M 2009 *J. Phys. Chem.* B **113** 15747–59

[32] Zhang J M *et al* 2001 *J. Phys. Chem.* A **105** 8878–91

[33] Philpott M R 1967 *J. Chem. Phys.* **47** 4437–45

[34] Spano F C 2010 *Acc. Chem. Res.* **43** 429–39

[35] Lim S-H, Bjorklund T G, Spano F C and Bardeen C J 2004 *Phys. Rev. Lett.* **92** 1–4

[36] Roden J, Schulz G, Eisfeld A and Briggs J 2009 *J. Chem. Phys.* **131** 044909

[37] Sanematu T 1977 *J. Phys. Soc. Japan* **43** 600–4

[38] Debreczeny M P, Sauer K, Zhou J and Bryant D A 1995 *J. Phys. Chem.* **99** 8412–9

[39] Debreczeny M P, Sauer K, Zhou J and Bryant D A 1995 *J. Phys. Chem.* **99** 8420–31

[40] Riter R R, Edington M D and Beck W F 1996 *J. Phys. Chem.* **100** 14198–205

[41] Riter R E, Edington M D and Beck W F 1997 *J. Phys. Chem.* B **101** 2366–71

[42] Homoelle B J, Edington M D, Diffey W M and Beck W F 1998 *J. Phys. Chem.* B **102** 3044–52

[43] Womick J M and Moran A M 2009 *J. Phys. Chem.* B **113** 15771–82

[44] Zhang J M, Zhao F L, Zheng X G, Wang H Z, Yang T-S, Hayashi M and Lin S H 1999 *J. Photochem. Photobiol.* B **53** 128–35

[45] Gillbro T, Sharkov A V, Kryukov I V, Khoroshilov E V, Kryukov P G, Fischer R and Scheer H 1993 *Biochim. Biophys. Acta* **1140** 321–6

[46] Womick J M, Miller S A and Moran A M 2009 *J. Phys. Chem.* B **113** 6630–9

[47] Lee H, Cheng Y-C and Fleming G R 2007 *Science* **316** 1462–5

[48] Womick J M, Miller S A and Moran A M 2010 *J. Chem. Phys.* **133** 024507

[49] Qian W and Jonas D M 2003 *J. Chem. Phys.* **119** 1611

[50] Farrow D A, Smith E R, Qian W and Jonas D M 2008 *J. Chem. Phys.* **129** 1–20

[51] Farrow D A, Qian W, Smith E R, Ferro A A and Jonas D M 2008 *J. Chem. Phys.* **128** 144510

[52] Smith E R and Jonas D M 2011 *J. Phys. Chem.* A **115** 4101–13

[53] Lepetit L, Chériaux G and Joffre M 1995 *J. Opt. Soc. Am.* B **12** 2467–74

[54] Gallagher S M, Albrecht A W, Hybl J D, Landin B L, Rajaram B and Jonas D M 1998 *J. Opt. Soc. Am.* B **15** 2338–45

[55] Brixner T, Mancal T, Stiopkin I V and Fleming G R 2004 *J. Chem. Phys.* **121** 4221–36

[56] Cheng Y C and Fleming G R 2008 *J. Phys. Chem.* B **112** 4254–60

[57] Palings I, van den Berg E M M, Lugtenburg J and Mathies R A 1989 *Biochemistry* **28** 1498–507

[58] Andel F III, Murphy J T, Haas J A, McDowell M T, van der Hoef I, Lugtenburg J, Lagarias J C and Mathies R A 2000 *Biochemistry* **39** 2667–76

[59] Fodor S P, Lagarias J C and Mathies R A 1990 *Biochemistry* **29** 11141–6

[60] Abramavicius D and Mukamel S 2004 *Chem. Rev.* **104** 2073–98

[61] Mukamel S 1995 *Principles of Nonlinear Optical Spectroscopy* (New York: Oxford University Press)

[62] Moran A M and Mukamel S 2004 *Proc. Natl Acad. Sci.* **101** 506–10

[63] McHale J 1999 *Molecular Spectroscopy* (Upper Saddle Creek River, NJ: Prentice-Hall)

[64] Frisch M J *et al* 2009 Gaussian 09, Revision C.01

[65] Dwyer J J, Gittis A G, Karp D A, Lattman E E, Spencer D S, Stites W E and Garcia-Moreno B 2000 *Biophys. J.* **79** 1610–20

[66] Ren Y, Wan J, Xu X, Zhang Z and Yang G 2006 *J. Phys. Chem.* B **110** 18665–9
[67] Albrecht A C 1961 *J. Chem. Phys.* **34** 1476–84
[68] Waterland M R, Stockwell D and Kelley A M 2001 *J. Chem. Phys.* **114** 6249–58
[69] Doust A B, Marai C N J, Harrop S J, Wilk K E, Curmi P M G and Scholes G D 2004 *J. Mol. Biol.* **344** 135–53
[70] Doust A B, Wilk K E, Curmi P M G and Scholes G D 2006 *J. Photochem. Photobiol.* A **184** 1–17
[71] Doust A B, van Stokkum I H M, Larsen D S, Wilk K E, Curmi P M G, van Grondelle R and Scholes G D 2005 *J. Phys. Chem.* B **109** 14219–26
[72] Book L D, Arnett D C, Hu H and Scherer N F 1998 *J. Phys. Chem.* A **102** 4350–9
[73] Wang X-Q, Li L-N, Chang W-R, Zhang J-P, Gui L-L, Guo B-J and Liang D-C 2001 *Acta Crystallogr. D* **57** 784–92
[74] Edington M D, Riter R E and Beck W F 1996 *J. Phys. Chem.* **100** 14206–17